Journal of Hepatocellular Carcinoma

Dovepress
Taylor & Francis Group

Open Access Full Text Article

ORIGINAL RESEARCH

Pleione bulbocodioides Polysaccharides Reprogram Tumor-Associated Macrophages via JAK2/STAT3 Inhibition to Suppress Hepatocellular Carcinoma

Yongjia Yang[1,2], Yujie Zhang[1,2], Xiaoyan Feng[2], Fen Gao[3], Yanhua Ma[1,2], Shaojun Yang[1,4]

[1]Key Laboratory of Dunhuang Medicine, Ministry of Education, Gansu University of Chinese Medicine, Lanzhou, Gansu, People's Republic of China; [2]The First Clinical Medical College, Gansu University of Chinese Medicine, Lanzhou, Gansu, People's Republic of China; [3]Clinical Medical College, Hubei College of Chinese Medicine, Jingzhou, Hubei, People's Republic of China; [4]Beihai Hospital of Traditional Chinese Medicine, Beihai, Guangxi, People's Republic of China

Correspondence: Yanhua Ma; Shaojun Yang, Email 617747928@qq.com; 3900316815@qq.com

Background: Tumor-associated macrophages (TAMs) are key regulators of the immunosuppressive tumor microenvironment in hepatocellular carcinoma (HCC). Sustained activation of the JAK2/STAT3 signaling pathway is closely associated with the maintenance of the pro-tumorigenic M2 macrophage phenotype. *Pleione bulbocodioides* polysaccharides (PBPs) have been reported to exhibit immunomodulatory and antitumor activities; however, whether PBPs regulate TAM polarization in HCC and the involvement of JAK2/STAT3 signaling remain unclear.

Methods: The monosaccharide composition and molecular-weight distribution of PBPs were first characterized. Their immunomodulatory effects were evaluated in vitro using IL-4/IL-13–induced M2-polarized RAW264.7 macrophages. In vivo, a Hepa1-6 tumor-bearing mouse model was established to assess the effects of PBPs on tumor growth, intratumoral macrophage composition, and JAK2/STAT3 signaling. The JAK2/STAT3 inhibitor AG490 was included as a pharmacological reference.

Results: PBPs were identified as high–molecular-weight polysaccharides predominantly composed of mannose and glucose and exhibited no cytotoxicity toward macrophages within the tested concentration range. In vitro, PBPs attenuated M2-associated marker expression and reduced the secretion of immunosuppressive cytokines, including interleukin-10 and transforming growth factor-β. In Hepa1-6 tumor-bearing mice, PBPs dose-dependently suppressed tumor growth and remodeled intratumoral macrophage composition, characterized by a decrease in M2 macrophages and a concomitant increase in M1 macrophages. These effects were accompanied by suppressed JAK2/STAT3 signaling and coordinated regulation of apoptosis- and angiogenesis-related factors.

Conclusion: PBPs suppress HCC progression in association with modulation of TAM polarization and inhibition of JAK2/STAT3 signaling. These findings provide mechanistic insight into the immunomodulatory actions of PBPs and support their further investigation as macrophage-targeting agents for HCC.

Keywords: *Pleione bulbocodioides* polysaccharides, macrophage polarization, JAK2/STAT3 signaling, hepatocellular carcinoma, tumor immune microenvironment

Introduction

Hepatocellular carcinoma (HCC), one of the most lethal malignancies worldwide, is characterized by a profoundly immunosuppressive tumor microenvironment that can compromise the efficacy of current systemic therapies such as immune checkpoint blockade.[1–3] Most HCC cases still exhibit intrinsic or acquired resistance, despite durable responses produced by immunotherapy in a subset of patients, underscoring the need for alternative strategies capable of reshaping immune suppression at the cellular and molecular levels.[4,5]

As a dominant immune population within the HCC microenvironment, tumor-associated macrophages (TAMs) are increasingly recognized to represent a major obstacle to effective antitumor immunity.[6,7] Rather than existing as discrete activation states, TAMs occupy a continuum of phenotypes. Notably, HCC tumors are preferentially enriched in

https://doi.org/10.2147/JHC.S578276
Received: 6 November 2025
Accepted: 13 February 2026
Published: 27 March 2026

macrophages exhibiting immunosuppressive, M2-like features.[8] These macrophages are known to support tumor progression by secreting mediators such as interleukin (IL)-10 and transforming growth factor-β (TGF-β), promoting angiogenesis, and suppressing antitumor immune responses.[9,10] Increasing evidence suggests that the persistence of this M2-skewed state, rather than macrophage abundance alone, represents a critical barrier to immune reprogramming in HCC.

At the molecular level, the Janus kinase 2/signal transducer and activator of transcription 3 (JAK2/STAT3) pathway has been implicated as an important regulator of macrophage polarization and tumor-associated inflammation.[11,12] Sustained activation of this pathway is thought to integrate cytokine-driven signals, particularly those mediated by IL-6, to reinforce M2-associated transcriptional programs while supporting tumor cell survival, angiogenesis, and immune evasion.[13–15] In contrast to transient inflammatory pathways (eg., NF-κB, MAPK, etc)., JAK2/STAT3 signaling is considered a relatively stable axis enabling macrophage-mediated immune suppression within the tumor microenvironment.[16] However, it remains unclear whether this pathway can be effectively modulated by naturally derived immunomodulators in HCC.

Pleione bulbocodioides (*P. bulbocodioides*) is a traditional medicinal herb that has garnered increasing attention for its anti-inflammatory and immunomodulatory properties.[17,18] *Pleione bulbocodioides* polysaccharides (PBPs) have been reported to exhibit antitumor activity in several experimental settings.[19] Nevertheless, their roles in regulating TAM polarization and the associated signaling mechanisms in the HCC microenvironment remain poorly defined. In particular, it is unclear whether PBPs attenuate M2-associated macrophage features by targeting pathways that stabilize immunosuppressive macrophage programs, such as JAK2/STAT3.

Accordingly, the present study was conducted to elucidate the immunomodulatory effects of PBPs on macrophage polarization using both in vitro and in vivo HCC models. By integrating compositional characterization with molecular and cellular analyses, this study aimed to examine the impact of PBPs on M2-associated macrophage features, intratumoral macrophage composition, and JAK2/STAT3 signaling activity. Collectively, these findings may provide insight into the mechanistic basis by which PBPs remodel the tumor immune microenvironment and inform macrophage-targeted immunomodulatory strategies in HCC.

Materials and Methods

Experimental Animals and Cell Lines

All animal procedures in this study were officially approved by the Ethics Committee of the Experimental Animal Center of Gansu University of Chinese Medicine (Approval No. SY2025-241). All animals experiments were conducted in accordance with the guidelines of the American Veterinary Medical Association. The experimental animals used in our study were male specific pathogen-free C57BL/6J mice (4–6 weeks old, 16–20 g) purchased from Chengdu Yaokang Biotechnology Co., Ltd. (Chengdu, China). Mice were housed under standard laboratory conditions (22 ± 2 °C, humidity of 50 ± 10%, and 12 h/12 h light/dark cycle), with ad libitum access to food and water.

Meanwhile, the experimental cell lines were murine RAW264.7 macrophages and murine HCC cell line Hepa1-6 from Suzhou Haixing Biotechnology Co., Ltd. (Suzhou, China). Cells were cultured in Dulbecco's modified Eagle's medium (DMEM) supplemented with 10% fetal bovine serum (FBS) and 1% penicillin–streptomycin in a humidified incubator containing 5% CO_2 at 37 °C. Prior to use, all cell lines were routinely tested for mycoplasma contamination and confirmed to be negative.

Reagents and Antibodies

PBPs (product code TDT203) (Shanghai Ronghe Pharmaceutical Technology Development Co., Ltd., Shanghai, China). Recombinant mouse IL-4 (cat. no. CK15) and IL-13 (cat. no. CH18) (Suzhou GenScript Biotech Corporation, Suzhou, China). Mouse IL-10 enzyme-linked immunosorbent assay (ELISA) kit (cat. no. JL20242) and mouse TGF-β ELISA kit (cat. no. JL13959) (Shanghai Jianglai Biotechnology Co., Ltd., Shanghai, China). FBS (cat. no. AUS-01S-02) (Cell-Box Biological Products Trading Co., Ltd., Hong Kong, China). DMEM (cat. no. SH30243.FS) (Cytiva, Logan, UT, USA). Penicillin–streptomycin solution (cat. no. P1400) and trypsin (cat. no. T1350) (Beijing Solarbio Science & Technology Co., Ltd., Beijing, China). RNA extraction kit (cat. no. AG21024), reverse transcription kit (cat. no. AG11728), and

SYBR Green qPCR Master Mix (cat. no. AG11718) (Accurate Biotechnology Co., Ltd., Changsha, China). The 10% PAGE precast gel kit (cat. no. AP15L535) (Heyuan Liji Biotechnology Co., Ltd., Shanghai, China). An enhanced chemiluminescence (ECL) ultra-sensitive detection kit (cat. no. 36208ES60) (Yeasen Biotechnology, Shanghai, China).

Fluorescein isothiocyanate-conjugated anti-F4/80 antibody (cat. no. 111602) (BioLegend San Diego, CA, USA). Phycoerythrin-conjugated anti-CD86 (cat. no. F2108602), Cy5.5-conjugated anti-CD11b (cat. no. F41011b04), and allophycocyanin-conjugated anti-CD206 (cat. no. F2120603) antibodies (Lianke Biotechnology Co., Ltd., Hangzhou, China). Primary antibodies against JAK2 (cat. no. AF6022), phospho-JAK2 (cat. no. AF3024), STAT3 (cat. no. AF6294), phospho-STAT3 (cat. no. AF3293), BCL-2 (cat. no. AF6139), and β-Actin (cat. no. AF7018) (Affinity Biosciences, Cincinnati, OH, USA). Polyvinylidene fluoride (PVDF) membranes (cat. no. PR05509) (Merck KGaA, Darmstadt, Germany). Goat Anti-Rabbit IgG (H+L) HRP (cat. no. S0001) (Affinity Biosciences, Cincinnati, OH, USA).

Main Instruments

The electrophoresis tank (HT-Zy03) and electrophoresis apparatus (HT-600C and HT-Mini) (Beijing Hongtao Jiyie Technology Development Co., Ltd., Beijing, China). A NanoDrop 2000C micro-spectrophotometer (Thermo Fisher Scientific, Waltham, MA, USA) for nucleic acid and protein quantification. TC-96/G/H(b)B thermal cycler (Hangzhou Bioer Technology Co., Ltd., Hangzhou, China) for reverse transcription. Microtome (D-315), tissue spreading system (YD-AB3), and cryo-embedding station (YD-6L) (Jinhua Yidi Medical Equipment Co., Ltd., Jinhua, China). KF-FL-005 system (Ningbo Jiangfeng Bioinformatics Technology Co., Ltd., Ningbo, China) for microscopic scanning. GelView 6000ProII imaging system (Guangzhou Boluteng Biotechnology Co., Ltd., Guangzhou, China) for capturing chemiluminescent signals.

Characterization of PBPs

Following acid hydrolysis, PBPs were subjected to monosaccharide composition analysis by high-performance anion-exchange chromatography (HPAEC). Then, the calibration curves were generated using standard monosaccharides, followed by quantitative analysis based on the peak areas.

Using a series of molecular weight standards, high-performance gel permeation chromatography (HPGPC) was employed to determine the molecular weight distribution of PBPs. After that, the retention time profiles were referenced to calculate the weight-average molecular weight (Mw), number-average molecular weight (Mn), and peak molecular weight (Mp).

In vitro Experiments

Induction of M2-Polarized Macrophages and PBPs Treatment

RAW264.7 macrophages in the logarithmic growth phase were seeded and stimulated with recombinant mouse IL-4 and IL-13 (20 ng/mL each) for 24 h to induce M2 polarization.[20,21] Untreated RAW264.7 cells cultured under identical conditions without cytokine stimulation were used as the control group. Following polarization, cells were thoroughly washed, and the cytokine-containing medium was replaced with fresh culture medium.

To evaluate the effects of PBPs on established M2-polarized macrophages, PBPs were subsequently added at the indicated concentrations for an additional 24 h. For dose–response analyses, PBPs were tested at concentrations of 100, 200, and 400 μg/mL. The concentration range used in vitro was determined with reference to previously published studies investigating the immunomodulatory effects of bioactive polysaccharides.[22,23] Based on this range, 200 μg/mL was selected as a representative mid-range concentration for subsequent mechanistic analyses.

Cell Viability Assay Using the Cell Counting Kit-8 (CCK-8)

RAW264.7 cells were seeded into 96-well plates at a density of 5×10^3 cells per well and incubated overnight to allow cell attachment. Cells were then treated with PBPs at concentrations ranging from 12.5 to 400 μg/mL for 24 h. Cell viability was assessed using the Cell Counting Kit-8 (CCK-8) according to the manufacturer's instructions. Absorbance was measured at 450 nm using a microplate reader. Each experimental condition was tested in triplicate, and cell viability was expressed as a percentage relative to the untreated control group.

Cytokine Measurement Using ELISA

The concentrations of interleukin-10 (IL-10) and transforming growth factor-β (TGF-β) in cell culture supernatants were quantified using commercial enzyme-linked immunosorbent assay (ELISA) kits in accordance with the manufacturers' protocols. Optical density was measured at 450 nm, and cytokine concentrations were calculated based on standard curves.

Quantitative Real-Time PCR (qRT-PCR) in vitro

Total RNA was extracted from RAW264.7 cells using an RNA extraction kit and reverse-transcribed into complementary DNA (cDNA). Quantitative real-time PCR was performed using SYBR Green chemistry. The mRNA expression levels of Arg-1 and CD206 were normalized to glyceraldehyde-3-phosphate dehydrogenase (GAPDH). Relative gene expression was calculated using the $2^{-\Delta\Delta Ct}$ method. Primer sequences are provided in Table 1.

Flow Cytometry in vitro

RAW264.7 cells were harvested, washed with phosphate-buffered saline, and stained with a fluorochrome-conjugated anti-CD206 antibody. Cells were gated based on forward- and side-scatter properties to exclude debris and aggregates. Data acquisition was performed using a flow cytometer, and the proportion of $CD206^+$ cells was analyzed using FlowJo software. The flow cytometry gating strategy is shown in Supplementary Figure 1.

In vivo Experiments

Hepa1-6 Tumor-Bearing Mouse Model and Treatment Protocol

Hepa1-6 murine hepatocellular carcinoma cells (2×10^6 cells suspended in 100 μL phosphate-buffered saline) were subcutaneously injected into the axillary region of mice to establish a tumor-bearing HCC model.[24] Tumor formation was confirmed by palpation approximately 3 days after inoculation.

A total of 45 tumor-bearing mice were randomly assigned, using a random number generator, to five experimental groups (n = 8 per group): model control, low-dose PBPs (75 mg/kg), medium-dose PBPs (150 mg/kg), high-dose PBPs (300 mg/kg), and AG490 (8 mg/kg). In addition, an age-matched healthy control group (n = 5; no tumor inoculation) was included for spleen index comparison only.

The dose of AG490 was selected based on previously published studies employing JAK2/STAT3 inhibition in murine tumor models.[25] The doses of PBPs (75, 150, and 300 mg/kg) were determined with reference to prior in vivo studies of bioactive polysaccharides in murine tumor and immunomodulation models.[26] A three-level graded dosing design (1/4×, 1/2×, and 1×) was adopted to facilitate evaluation of dose–response effects. PBPs were administered once daily by oral

Table 1 List of qPCR Primers Used

Gene	Forward/Reverse Sequence (5′ to 3′)	Primer Length (bp)
CD206	TGGAGGGTGCGGTACACTAA	192
	CTGTTCTGACTCTGGACACTTGC	
Arg-1	CCAATGAAGAGCTGGCTGGTG	89
	AACTGCCAGACTGTGGTCTCC	
iNOS	GGACGAGACGGATAGGCAGA	120
CD86	ACATGCAAGGAAGGGAACTCT	130
JAK2	ATATGACCGTTGTGTGTGTTCTGGA	81
STAT3	AGGGCCACAGTAACTGAAGCTGTAA	135
	AGGCAACCTCCACATCTCCTG	
	GGACTGGCTCTATCTGCTTCACA	
	ACGAAAGTCAGGTTGCTGGT	
	TGTGTTCGTGCCCAGAATGT	
GAPDH	GGTTGTCTCCTGCGACTTCA	183
	TGGTCCAGGGTTTCTTACTCC	

gavage, whereas AG490 was administered by intraperitoneal injection. Treatments were continued for 14 consecutive days.

Investigators responsible for tumor measurement and data analysis were blinded to group allocation. Tumor length and width were measured using digital calipers, and tumor volume was calculated using the formula: $V = (\text{length} \times \text{width}^2)/2$. Tumor index was defined as tumor weight/body weight × 100%. The maximum allowable tumor volume did not exceed 1,500 mm^3.

Given the absence of reliable estimates of effect size and variance, this study did not calculate a priori sample size. As a result, the group size was determined based on prior murine tumor studies of similar design and feasibility considerations.[27,28]

Histological Analysis with Hematoxylin and Eosin (H&E) Staining

Tumor tissues were fixed in 4% paraformaldehyde, embedded in paraffin, sectioned at 4 μm, and stained with H&E. Finally, histopathological changes were examined under a light microscope.

qRT-PCR in vivo

qRT-PCR was performed following total RNA extraction from tumor tissues and reverse transcription into cDNA. The expression levels of Arg-1, CD206, CD86, iNOS, JAK2, and STAT3 were assessed and normalized to GAPDH. Similarly, the relative expression was calculated using the $2^{-\Delta\Delta Ct}$ method. Primer sequences are provided in Table 1.

Flow Cytometry in vivo

Tumor tissues were mechanically dissociated into single-cell suspensions. Cells were first gated based on forward- and side-scatter properties to exclude debris, followed by singlet discrimination. For flow cytometric analysis, 7-aminoactinomycin D (7-AAD) was used as a gating marker to exclude debris and non-specific events. Macrophages were identified as $CD11b^+F4/80^+$ cells within the gated population. M1-like macrophages were defined as $CD86^+$ cells, whereas M2-like macrophages were defined as $CD206^+$ cells. Data were acquired using a flow cytometer and analyzed using FlowJo software. The detailed flow cytometry gating strategy is provided in Supplementary Figure 2.

Western Blot

Extraction of the total protein from tumor tissues was completed using RIPA lysis buffer. Equal amounts of protein (30 μg per lane) were separated on 10% SDS-PAGE gels and transferred onto PVDF membranes. Membranes after sealing were subjected to incubation with HRP-conjugated anti-rabbit secondary antibodies following incubation with rabbit-derived primary antibodies (1:1000 dilution) at 4 °C for 8 h. Immunoreactive bands were detected using ECL and captured with a GelView 6000 Pro imaging system. Band intensities were quantified using ImageJ software. Phosphorylated proteins were normalized to their corresponding total proteins, and the total protein levels were normalized to β-actin.

Data Analysis

Statistical analyses were performed using GraphPad Prism software. All data are presented as mean±standard deviation (SD). Following testing for normality and homogeneity of variance, all data were analyzed by one-way analysis of variance (ANOVA) followed by Tukey's multiple comparisons test for determining muti-group differences. A P-value < 0.05 was considered statistically significant. The number of biological replicates (n) is indicated in the figure legends.

For in vitro cell-based experiments, all assays were performed using at least three independent biological replicates, with technical replicates as indicated. For downstream molecular and cellular analyses of tumor tissues in in vivo experiments (eg., qRT-PCR, Western blot, and flow cytometry), samples from three randomly selected mice per group were used as independent biological replicates.

Results

Monosaccharide Composition and Molecular Weight Distribution of PBPs

According to the HPAEC analysis, PBPs were predominantly composed of mannose and glucose, with minor amounts of galactose and galacturonic acid (Table 2).

HPGPC (Table 3) identified three major molecular-weight fractions, dominated by a high–molecular-weight fraction (Mw ≈ 135.6 kDa). Therefore, PBPs mainly consisted of macromolecular polysaccharide components.

In vitro Experiments

PBPs Did Not Affect the Viability of RAW264.7 Cells and M2-Polarized Macrophages

PBPs at varied concentrations (12.5–400 μg/mL) were used to treat RAW264.7 cells and IL-4/IL-13–induced M2-polarized macrophages for 24 h. Cell viability assays showed no significant changes in macrophage viability across the tested concentration range (Figure 1). Consequently, subsequent in vitro experiments were conducted within this concentration range.

PBPs Reduced Arg1 and CD206 mRNA Expression in M2-Polarized Macrophages

Consistent with the induction of an M2-polarized state, Arg1 and CD206 mRNA expression levels were increased in RAW264.7 macrophages after IL-4/IL-13 stimulation. Conversely, PBP treatment led to reduced Arg1 and CD206 transcript levels. Meanwhile, PBPs decreased Arg1 and CD206 mRNA expression in a concentration-dependent manner over the range of 100–400 μg/mL, showing consistent effects observed at 200 μg/mL (Figure 2).

PBPs Decreased CD206 Surface Expression in M2-Polarized Macrophages

Based on the results of flow cytometry, compared with the model group, PBP treatment reduced the proportion of CD206-positive macrophages. The greatest reduction in CD206-positive cells was observed at a PBP concentration of 200 μg/mL (Table 4 and Figure 3).

Table 2 Monosaccharide Composition of PBPs

Monosaccharide Composition Analysis	Content (μg/mg)
Fucose	0.00
Galactosamine Hydrochloride	0.00
Rhamnose	0.00
Arabinose	0.00
Glucosamine Hydrochloride	0.00
Galactose	13.58
Glucose	213.14
Xylose	0.00
Mannose	340.64
Fructose	0.00
Ribose	0.00
Galacturonic Acid	12.92
Guluronic Acid	0.00
Glucuronic Acid	0.00
Mannuronic Acid	0.00

Table 3 Molecular Weight Determination of PBPs

RT (min)	Mp (Da)	Mw (Da)	Mn (Da)	Peak area (%)
33.021	137,556	135,646	132,523	78.06
38.133	16,166	16,188	15,685	10.72
44.083	1388	1363	1308	11.22

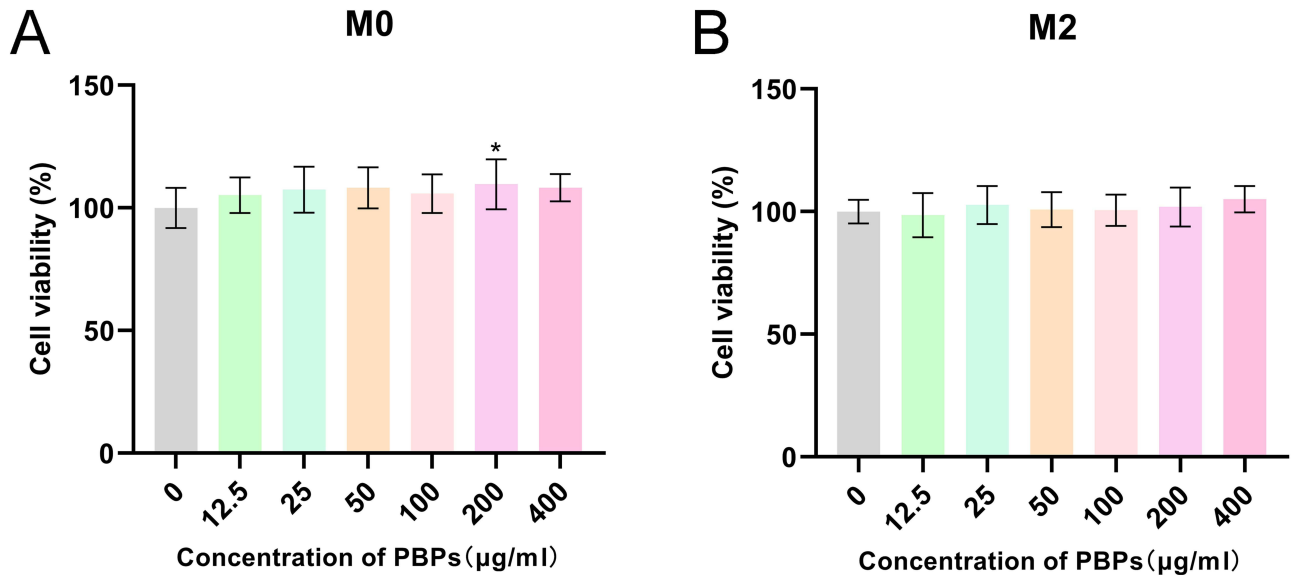

Figure 1 Effects of PBPs on RAW264.7 cell viability. (**A**) RAW264.7 cells treated with PBPs (0–400 μg/mL) for 24 h. (**B**) M2-polarized RAW264.7 cells (pre-treated with IL-4/IL-13 for 24 h) exposed to PBPs for an additional 24 h. Viability was assessed in both cases. Data are presented as mean ± SD (n = 3).
Note: Compared with the Control group *:P<0.05.

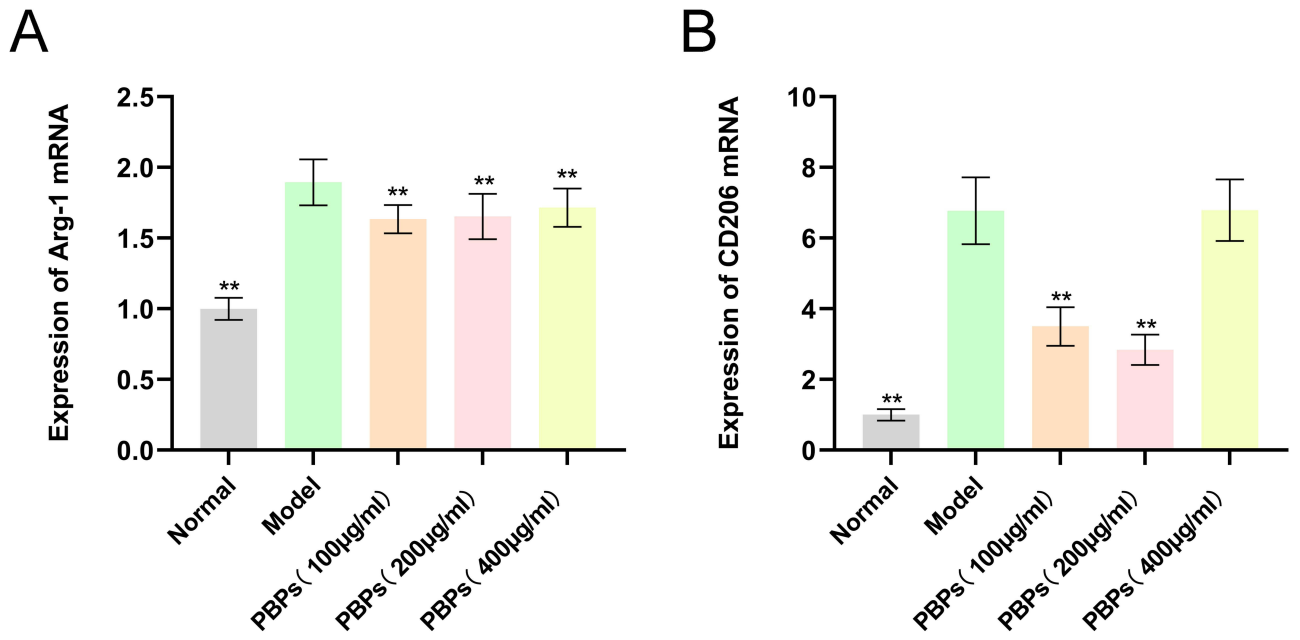

Figure 2 Effects of PBPs on reducing M2 marker gene expression in RAW264.7 macrophages. (**A**) Arg1 mRNA expression; (**B**) CD206 mRNA expression after 24 h of PBP treatment (100–400 μg/mL). Data are presented as mean ± SD (n = 3).
Note: Compared with the Model group **: P<0.01.

PBPs Reduced IL-10 and TGF-β Secretion in M2-Polarized Macrophages

ELISA of culture supernatants demonstrated significantly reduced secretion of the immunosuppressive cytokines IL-10 and TGF-β in M2-polarized macrophages following the exposure to PBPs. Therefore, PBPs could functionally attenuate the M2 phenotype (Figure 4).

https://doi.org/10.2147/JHC.S578276

Table 4 Proportion of $CD206^{+}$ Macrophages After PBPs Treatment

Group Tranches	The Proportion of M2-type Macrophages (%)
Normal	23.70 ± 1.42**
Model	32.27 ± 0.64
PBPs (100 μg/mL)	28.47 ± 1.08**
PBPs (200 μg/mL)	24.17 ± 0.47**
PBPs (400 μg/mL)	26.43 ± 0.50**

Note: Compared with Model group ** $P<0.01$.

In vivo Experiments

PBPs Reduced Tumor Burden and Altered Spleen Index in Hepa1-6 Tumor-Bearing Mice

In the Hepa1-6 tumor-bearing mouse model, the administration of PBPs resulted in a dose-dependent reduction in tumor index. Moreover, compared with the model group, high-dose PBPs and the JAK2/STAT3 inhibitor AG490 produced greater reductions in tumor index, whereas medium-dose PBPs showed intermediate effects (Figure 5A).

Furthermore, tumor-bearing mice had higher spleen index than in age-matched healthy mice. In addition, high-dose PBPs further increased the spleen index when compared to the model group (Figure 5B).

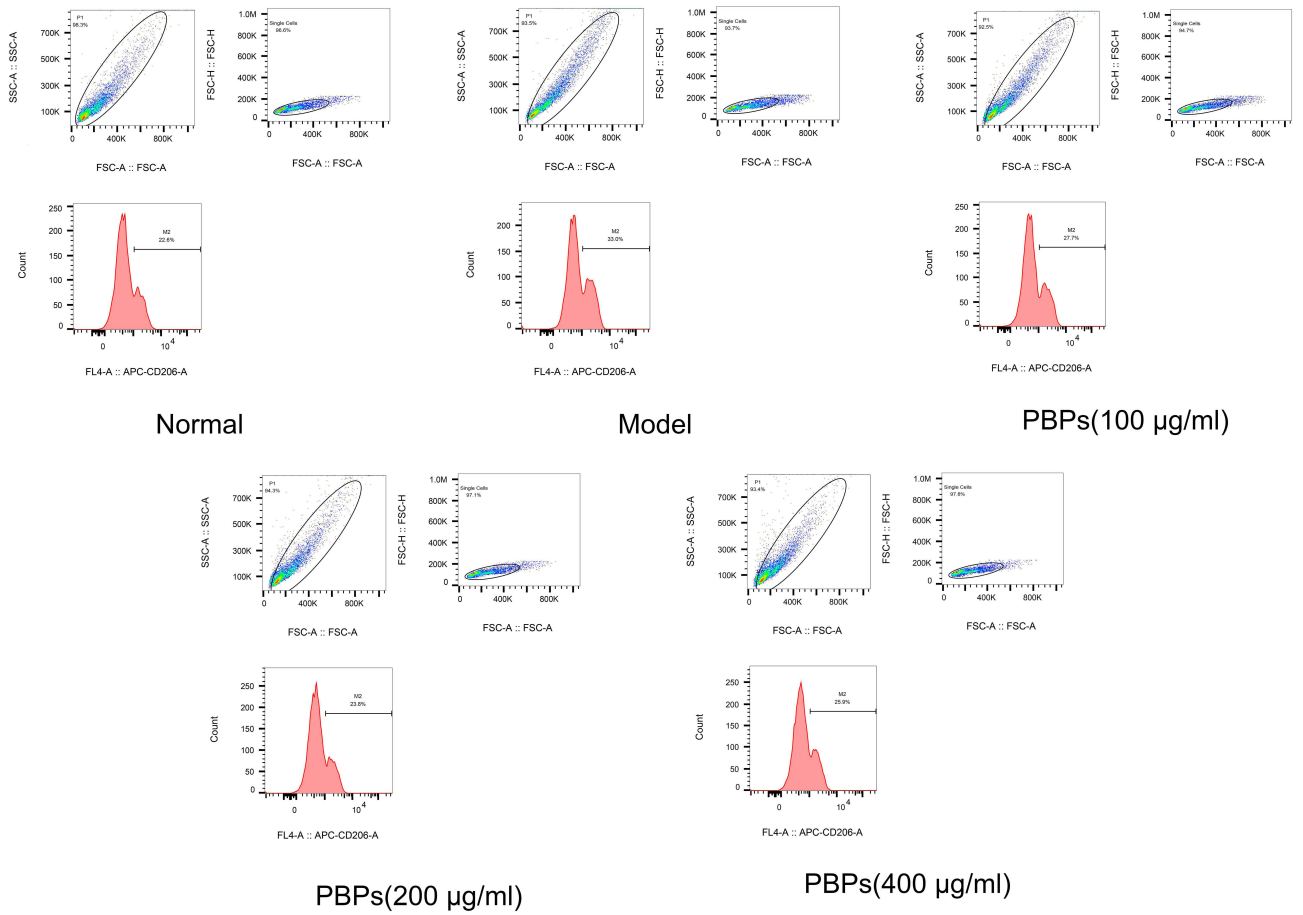

Figure 3 The effect of PBPs on downregulating CD206 surface expression in M2 macrophages. Representative flow cytometry histograms after 24 h of exposure to PBPs (100–400 μg/mL). Quantitative analysis of CD206-positive cells is provided in Table 4. Data are presented as mean ± SD (n = 3).
Note: Compared with the Model group **: P<0.01.

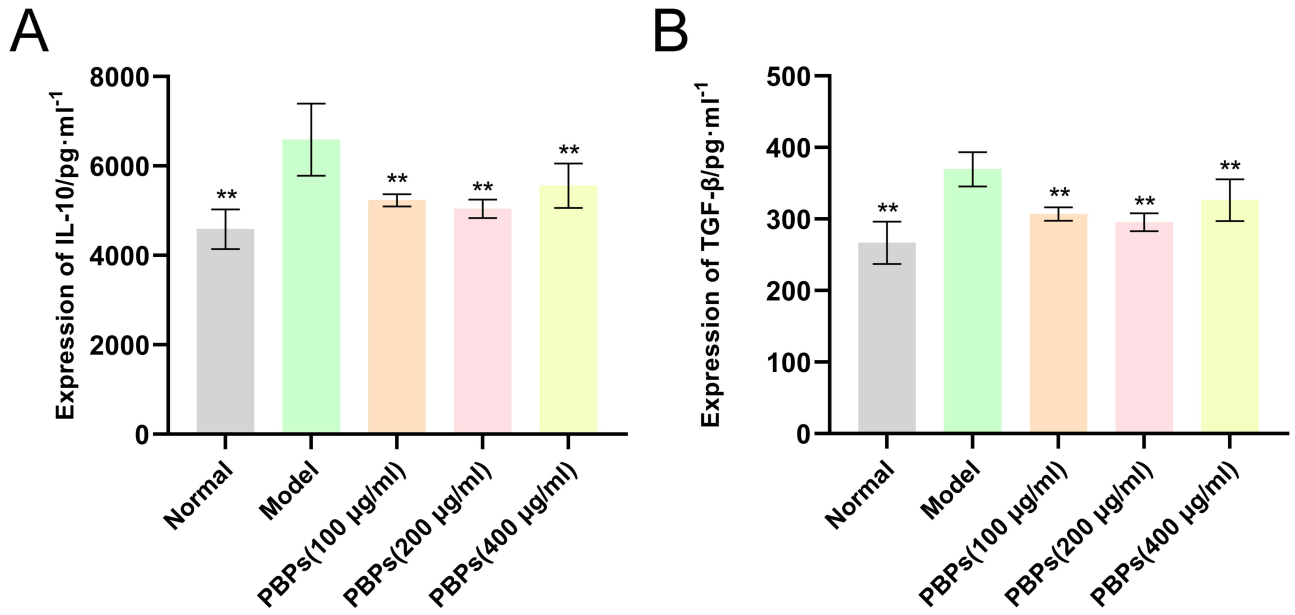

Figure 4 The effect of PBPs on suppressing immunoregulatory cytokine release in M2 macrophages. (**A**) IL-10 concentration; (**B**) TGF-β concentration after 24 h of treatment with PBPs (100–400 μg/mL). Data are presented as mean ± SD (n = 3).
Note: Compared with the Model group **: P<0.01.

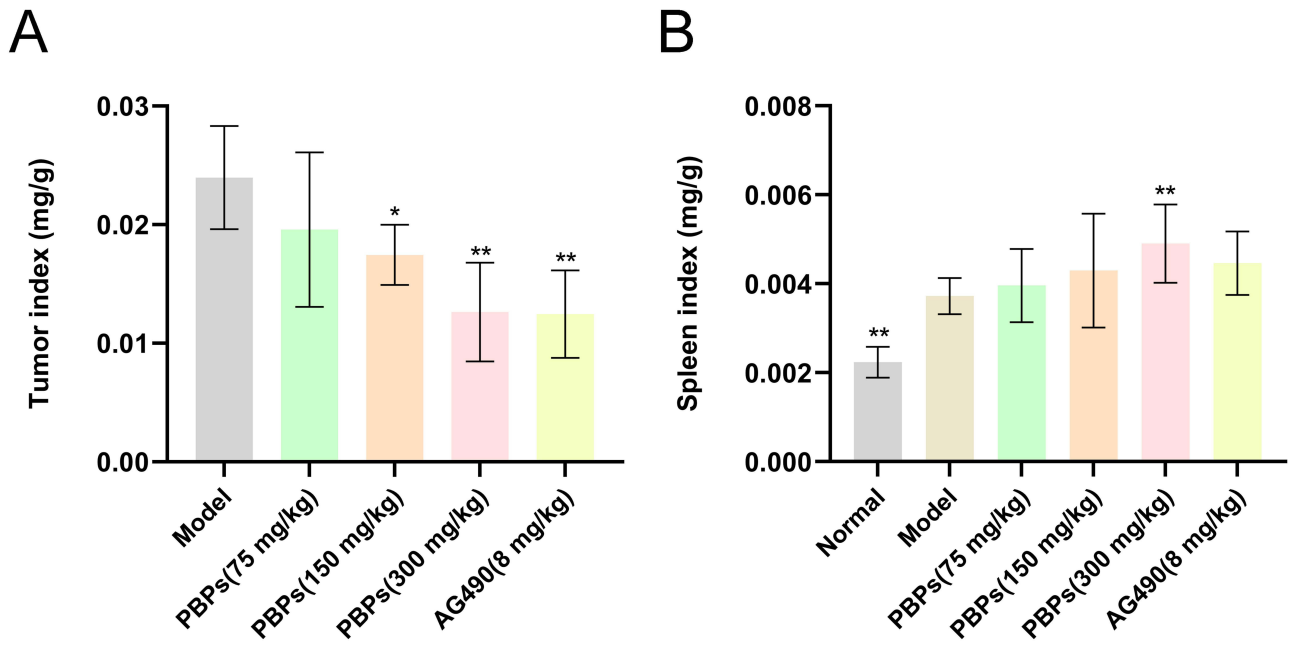

Figure 5 Effects of PBPs on tumor and spleen indices. (**A**) Tumor index after 14 days of PBP treatment (75–300 mg/kg/day) or AG490 treatment in Hepa1-6 tumor-bearing mice. (**B**) Spleen index measured in tumor-bearing mice under the same conditions, with age-matched healthy mice included as a control. Data are presented as mean ± SD (n = 8 per group).
Note: Compared with the Model group *: P<0.05; and **: P<0.01.

Histopathological Changes in Tumor Tissues Following PBPs Treatment

In accordance with the results of H&E staining, disorganized cellular architecture, frequent mitotic figures, basophilic cytoplasm, and areas of necrosis and fibrosis were observed in tumor tissues from model mice. In contrast, reduced mitotic activity and smaller necrotic areas were noticed in tumor tissues from mice exposed to high-dose PBPs or AG490 (Figure 6).

https://doi.org/10.2147/JHC.S578276

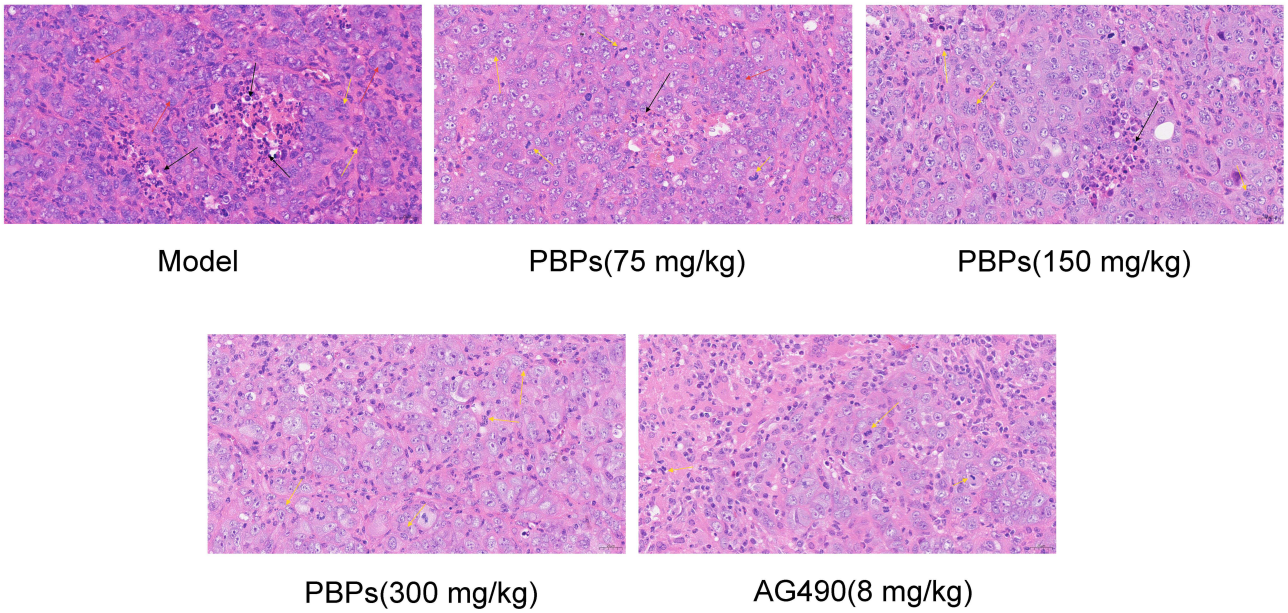

Figure 6 Representative H&E-stained tumor sections (×400). Yellow arrows: mitotic figures; red arrows: basophilic cytoplasm; and black arrows: necrotic/fibrotic areas.

PBPs Modulated Macrophage Polarization Markers and JAK2/STAT3 Transcripts in Tumor Tissues

qRT-PCR showed that high-dose PBPs reduced mRNA expression of JAK2, STAT3, as well as Arg-1 and CD206 (two M2-associated markers) in tumor tissues. Conversely, there was increased expression of CD86 and iNOS, two M1-associated markers. Similar expression patterns were observed in the AG490-treated group (Figure 7).

PBPs Reshaped Intratumoral Macrophage Composition

As evidenced by flow cytometry of tumor-infiltrating immune cells, the proportion of M2 macrophages was reduced, while that of M1 macrophages was increased in a dose-dependent manner after treatment with PBPs. Additionally, comparable changes were observed in the AG490-treated group (Table 5 and Figure 8).

PBPs Inhibited JAK2/STAT3 Activation and Regulated Apoptosis- and Angiogenesis-Related Proteins

Western blot showed that high-dose PBPs reduced the phosphorylation of JAK2 and STAT3 in tumor tissues. PBP treatment also upregulated the expression of BAX (a pro-apoptotic protein), and downregulated the expression of BCL-2 (a anti-apoptotic protein) and VEGF (an angiogenesis-related protein). Similar protein expression patterns were observed in the AG490-treated group (Figure 9).

Discussion

TAMs are increasingly recognized as key determinants of immune suppression and therapeutic resistance in HCC.[29,30] In this work, PBPs were found to attenuate M2-associated macrophage features, remodel intratumoral macrophage composition, and suppress tumor growth in vivo. In parallel, there was reduced activity of the JAK2/STAT3 pathway, a phenomenon that has been implicated in macrophage polarization and tumor-promoting inflammation.[14,31]

Consistently, PBPs suppressed M2-associated characteristics across experimental systems. In vitro, PBPs reduced expression of canonical M2 markers and decreased secretion of immunosuppressive cytokines (eg., IL-10 and TGF-β) in IL-4/IL-13–induced macrophages under non-cytotoxic conditions. Consistent with attenuation of M2-associated programs, rather than binary repolarization, these changes were observed without evidence of complete conversion toward an M1 phenotype. In line with current views, this pattern indicates that macrophage polarization represents a continuum of functional states, instead of discrete endpoints.

In vivo, PBP treatment was associated with the remodeling of the tumor immune microenvironment, characterized by reduced prevalence of M2 macrophages and relatively increased M1-associated populations within tumor tissues. These

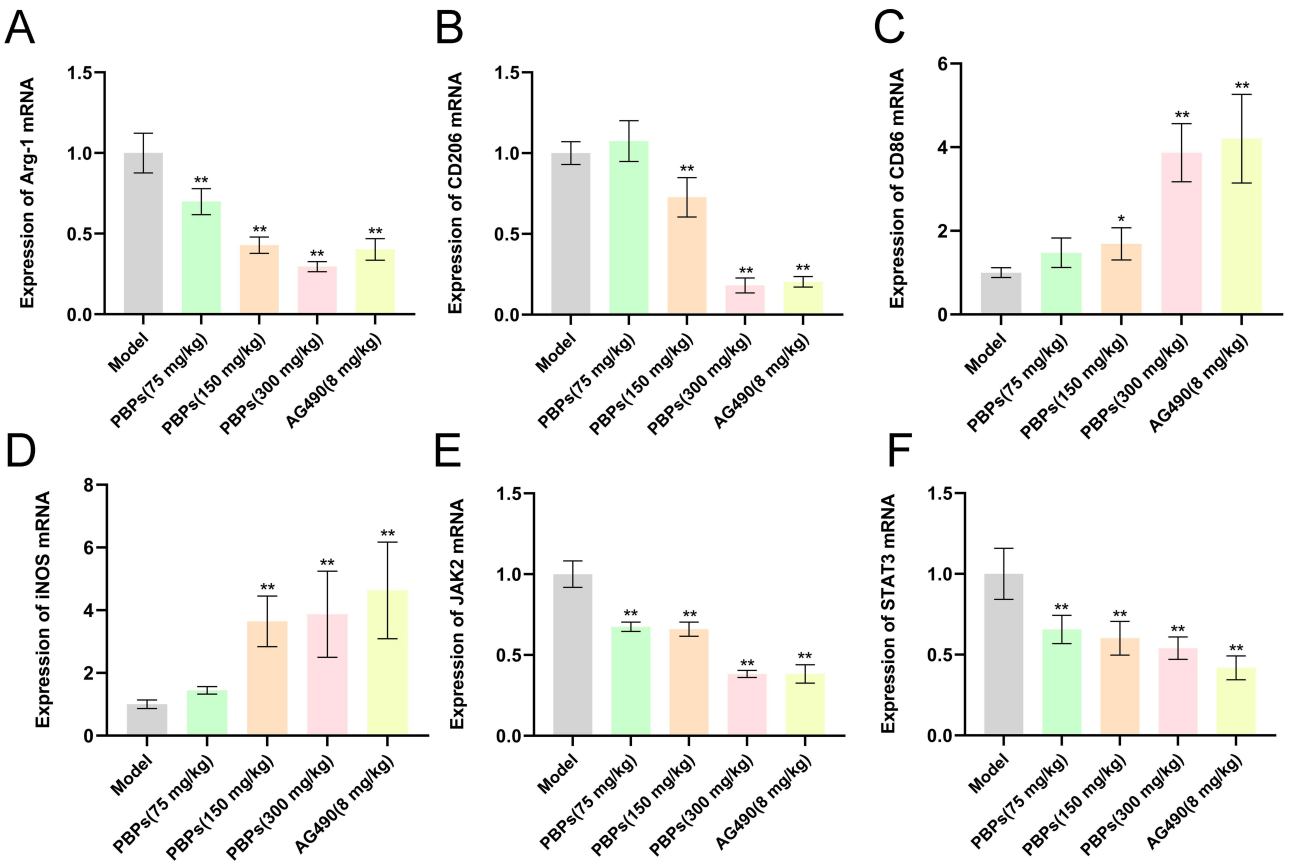

Figure 7 Effects of PBPs on modulating macrophage polarization and the expression of genes related to the JAK2/STAT3 pathway in tumors. (**A** and **B**) M2 markers (Arg-1, and CD206); (**C** and **D**) M1 markers (CD86, and iNOS); (**E** and **F**) JAK2 and STAT3 transcripts. Data are presented as mean ± SD (n = 3).
Note: Compared with the Model group *: P<0.05; and **: P<0.01.

immunological changes occurred alongside reduced tumor burden and improved histopathological features, supporting a functional relationship between macrophage composition and tumor progression. The administration of PBPs was also associated with elevated spleen index. In tumor-bearing models, alterations in spleen index have been reported frequently in the context of immune modulation induced by immunotherapeutic or immunomodulatory interventions, including bioactive polysaccharides. However, the immunological basis of this observation requires further cellular and functional characterization given that changes in spleen index may also reveal tumor-driven extramedullary hematopoiesis or expansion of immunosuppressive myeloid populations.[32] In mice treated by AG490, a JAK2/STAT3 inhibitor, there were comparable antitumor and immunological effects, supporting the involvement of this pathway in the observed responses.[33–35]

The JAK2/STAT3 pathway has been documented to regulate immunosuppressive macrophage phenotypes and tumor-associated inflammation.[36–38] PBP treatment was associated with reduced activation of JAK2/STAT3 signaling, together

Table 5 Percentages of M1 and M2 Macrophages in Tumors Following PBPs Treatment

Group Tranches	The Proportion of M1-Type Macrophages (%)	The Proportion of M2-Type Macrophages (%)
Model	2.71 ± 0.49	15.73 ± 4.79
PBPs (75 mg/kg)	3.92 ± 0.67	2.30 ± 1.22**
PBPs (150 mg/kg)	4.87 ± 0.55	0.76 ± 0.49**
PBPs (300 mg/kg)	6.16 ± 1.35**	0.58 ± 0.27**
AG490 (8 mg/kg)	10.31 ± 1.50**	1.77 ± 1.37**

Note: Compared with Model group ** *P*<0.01.

https://doi.org/10.2147/JHC.S578276

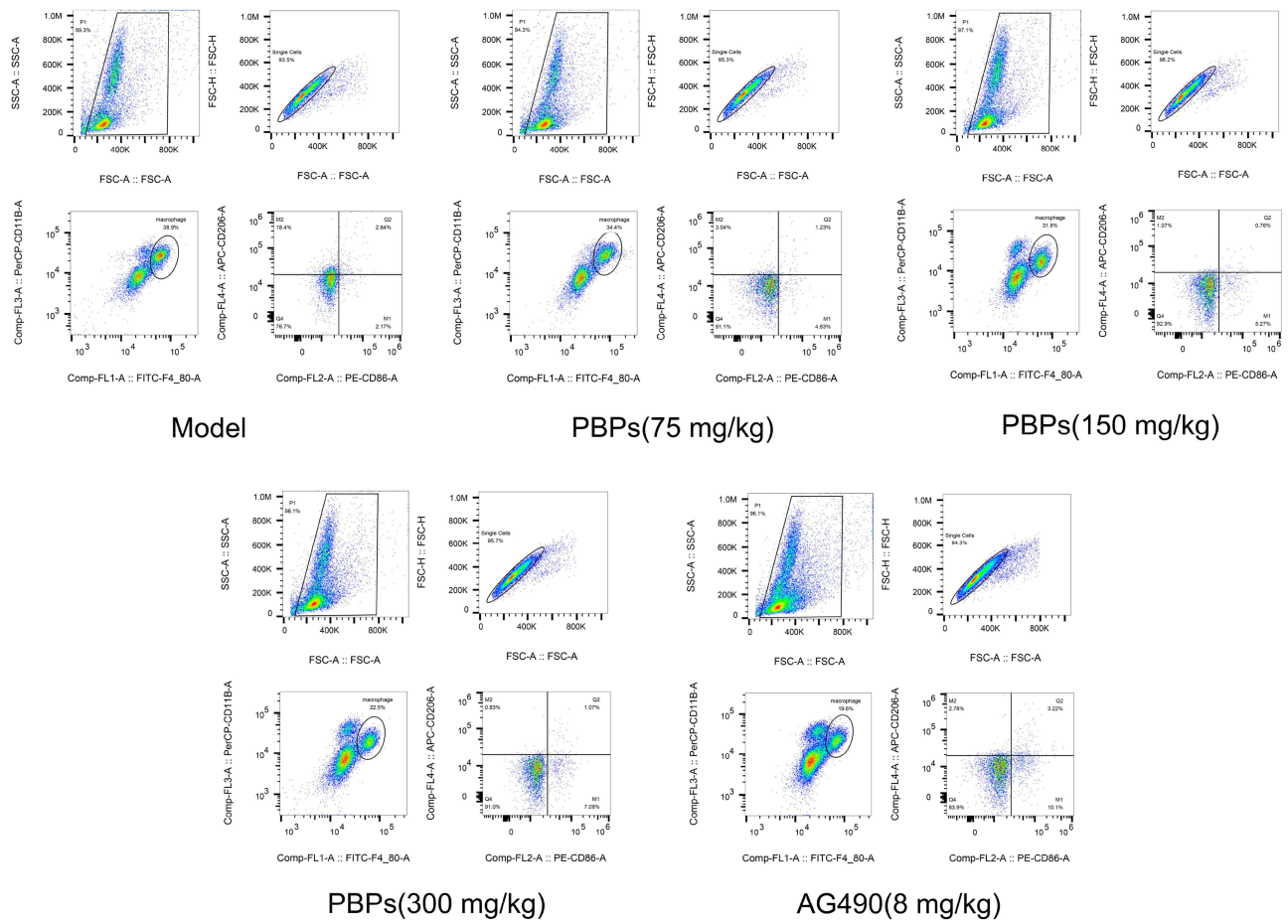

Figure 8 Effects of PBPs on promoting M1 and suppressing M2 macrophage prevalence in tumors. Representative flow cytometry plots of tumor-infiltrating macrophages after PBP or AG490 treatment. Macrophages were gated as $CD11b^{+}F4/80^{+}$ cells; M1 macrophages were defined as $CD86^{+}$ cells and M2 macrophages as $CD206^{+}$ cells. Quantitative analysis is provided in Table 5. Data are presented as mean ± SD (n = 3).
Note: Compared with the Model group *: P<0.05; and **: P<0.01.

with coordinated regulation of apoptosis- and angiogenesis-related proteins, including BAX, BCL-2, and VEGF. The proposed axis would be dampened, beyond phosphorylation-dependent regulation, as evidenced by the reduction in both the phosphorylated and total JAK2/STAT3 levels. Such patterns are compatible with the engagement of endogenous negative-feedback mechanisms, including SOCS-mediated JAK degradation, STAT3 proteasomal turnover, and attenuation of IL-6/gp130-driven feed-forward signaling.[39,40] These molecular changes provide a mechanistic framework for the suppressed tumor growth observed in our study. Nevertheless and critically, the present findings establish potential association, rather than direct causality, despite the presence of pathway involvement as supported by the parallel effects of PBPs and AG490.

Currently, a series of recognized polysaccharides can exert immunomodulatory or antitumor effects predominantly through canonical inflammatory pathways, particularly NF-κB and MAPK signaling.[22,41,42] Polysaccharides derived from *Ganoderma lucidum* and *Astragalus membranaceus*, for example, enable the regulation of the activation of macrophages and the release of inflammatory cytokines primarily via NF-κB- and MAPK-dependent mechanisms, presenting a common paradigm in polysaccharide research.[43–47] In contrast, comparatively fewer studies have centered on the JAK2/STAT3 axis in the context of macrophage polarization, despite its established role in sustaining M2-associated transcriptional programs. Meanwhile, several studies exploring the effect of some polysaccharides on STAT3 phosphorylation rarely position JAK2/STAT3 as a macrophage-centered regulatory axis or integrate phenotypic, signaling, and in vivo validation. On the basis of the above, the present findings established a link of PBP-mediated

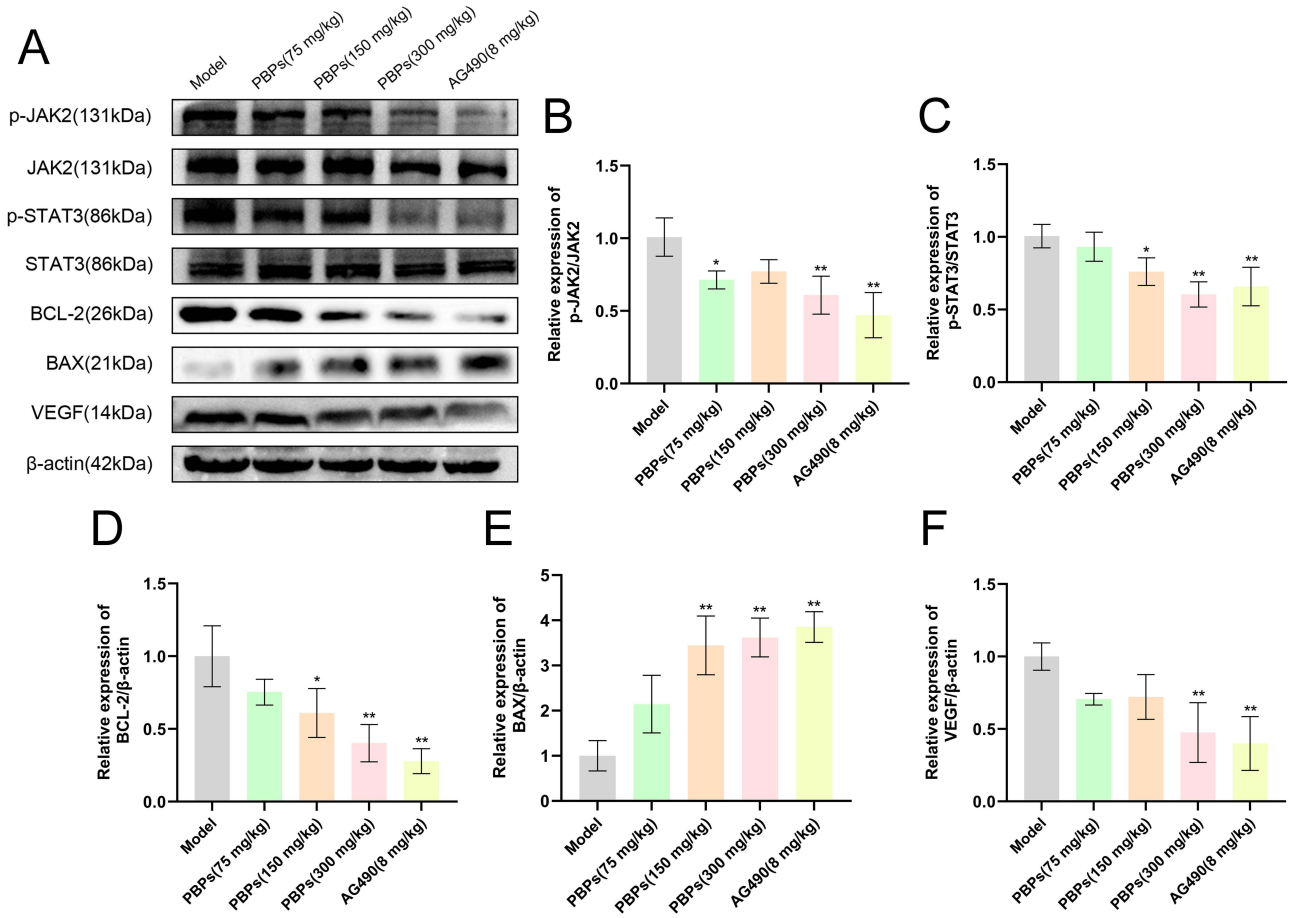

Figure 9 Effects of PBPs on regulating protein expression related to JAK2/STAT3 signaling, apoptosis, and angiogenesis in tumors. (**A**) Representative Western blot images; (**B**) p-JAK2/JAK2; (**C**) p-STAT3/STAT3; (**D**) BCL-2; (**E**) BAX; (**F**) VEGF. Data are presented as mean ± SD (n = 3).
Note: Compared with the Model group *: P<0.05; and **: P<0.01.

immunomodulation to a JAK2/STAT3 signaling axis governing macrophage polarization, with AG490 selected as a pathway-matched pharmacological reference.

PBPs were identified as high–molecular-weight polysaccharides predominantly composed of mannose and glucose. At present, polysaccharides with similar compositional features have been associated with immunomodulatory activity, our study, however, fail to resolve linkage patterns, branching structures, or receptor interactions responsible for the bioactivity of PBPs.[48,49] Consequently, this study merely yielded speculative evidence on the potential engagement of mannose receptors or other pattern recognition receptors, necessitating dedicated structural and receptor-level investigation.

A strength of this study is the construction of an integrative experimental framework, combining in vitro macrophage polarization assays with in vivo tumor-bearing models to generate convergent immunological and therapeutic evidence within a macrophage-centered mechanistic context. Simultaneously, this study ensured internal consistency across molecular, cellular, and tissue-level readouts through the use of multiple analytical platforms, including qRT-PCR, Western blot, and flow cytometry. Furthermore, dose–response analyses supported the robustness of the observed effects and facilitated the interpretation of PBP activity within a defined experimental window.

Nevertheless, this study still has several limitations. Firstly, our mechanistic analyses emphasized on macrophage polarization markers and JAK2/STAT3 signaling within a single murine HCC model. Additional investigation is needed to extend these findings to other immune compartments, tumor models, and translational parameters such as pharmacokinetics and toxicology. Secondly, this study failed to directly examine the functional properties of macrophages, including phagocytic capacity, effector functions, or direct tumor cell interactions, despite systematic assessment of

https://doi.org/10.2147/JHC.S578276

macrophage phenotypic markers and cytokine profiles. Furthermore, given that most measurements were performed at the experimental endpoint, it remained unresolved regarding the temporal relationships among JAK2/STAT3 modulation, macrophage reprogramming, and tumor suppression. In addition, this study did not carry out systemic immune profiling in non–tumor-bearing animals, even with age-matched healthy mice included as a control for spleen index assessment.

Collectively, PBPs can modulate macrophage-driven immune suppression in HCC, with JAK2/STAT3 signaling identified as a key molecular correlate of this process. This study demonstrates the roles of PBPs, a type of naturally derived polysaccharide fraction, in remodeling the tumor immune microenvironment and suppressing tumor progression in vivo, supporting macrophage-targeted immunomodulation as a complementary anti-HCC strategy.

Conclusion

In summary, PBPs can modulate the macrophage compartment within the HCC microenvironment and suppress tumor progression in vivo. PBPs can attenuate M2-associated macrophage features, and reshape intratumoral macrophage composition, which are associated with the inactivation of JAK2/STAT3 signaling as well as coordinated regulation of apoptosis- and angiogenesis-related pathways. This study demonstrates the immunomodulatory activity of PBPs in HCC, encouraging the feasibility of targeting TAM-driven immune suppression through non-cytotoxic immunomodulatory strategies. In the future, additional efforts should be made to define the structure–activity relationships and upstream sensing receptors of PBPs, establish the causal role of JAK2/STAT3 signaling using macrophage-specific approaches, and validate these effects in other HCC models and in combination with existing systemic therapies.

Data Sharing Statement

The data that support the findings of this study are available from the corresponding authors, Yanhua Ma and Shaojun Yang, upon reasonable request.

Author Contributions

All authors made a significant contribution to the work reported, whether that is in the conception, study design, execution, acquisition of data, analysis and interpretation, or in all these areas; took part in drafting, revising or critically reviewing the article; gave final approval of the version to be published; have agreed on the journal to which the article has been submitted; and agree to be accountable for all aspects of the work.

Funding

This work was supported by the General Project of the Gansu Province Joint Scientific Research Fund (grant no. 23JRRA1523, to Yanhua Ma) and the Open Fund of the Key Laboratory of Dunhuang Medicine and Transformation, Ministry of Education (grant no. DHYX21-04, to Shaojun Yang).

Disclosure

The authors declare that they have no known competing financial interests or personal relationships that could have appeared to influence the work reported in this paper.

References

1. Wang X, Zhang Q, Zhou J, et al. T cell-mediated targeted delivery of tadalafil regulates immunosuppression and polyamine metabolism to overcome immune checkpoint blockade resistance in hepatocellular carcinoma. *J Immunother Cancer*. 2023;11:e006493. doi:10.1136/jitc-2022-006493
2. Sheta E, El-Kalla F, El-Gharib M, et al. Comparison of single-session transarterial chemoembolization combined with microwave ablation or radiofrequency ablation in the treatment of hepatocellular carcinoma: a randomized-controlled study. *Eur J Gastroenterol Hepatol*. 2016;28:1198–1203. doi:10.1097/MEG.0000000000000688
3. Elwan N, Salem ML, Kobtan A, et al. High numbers of myeloid derived suppressor cells in peripheral blood and ascitic fluid of cirrhotic and HCC patients. *Immunol Invest*. 2018;47(2):169–180. doi:10.1080/08820139.2017.1407787
4. Wang H, Liang Y, Liu Z, et al. POSTN + cancer-associated fibroblasts determine the efficacy of immunotherapy in hepatocellular carcinoma. *J Immunother Cancer*. 2024;12:e008721. doi:10.1136/jitc-2023-008721
5. Chen J, Feng W, Sun M, et al. TGF-β1-induced SOX18 elevation promotes hepatocellular carcinoma progression and metastasis through transcriptionally upregulating PD-L1 and CXCL12. *Gastroenterology*. 2024;167:264–280. doi:10.1053/j.gastro.2024.02.025

6. Chiu DK-C, Zhang X, Cheng BY-L, et al. Tumor-derived erythropoietin acts as an immunosuppressive switch in cancer immunity. *Science*. 2025;388:eadr3026. doi:10.1126/science.adr3026
7. Zhang F, Jiang Q, Cai J, et al. Activation of NOD1 on tumor-associated macrophages augments CD8 + T cell–mediated antitumor immunity in hepatocellular carcinoma. *Sci Adv*. 2024;10(40):eadp8266. doi:10.1126/sciadv.adp8266
8. Yang C-L, Song R, Hu J-W, et al. Integrating single-cell and bulk RNA sequencing reveals CK19 + cancer stem cells and their specific SPP1 + tumor-associated macrophage niche in HBV-related hepatocellular carcinoma. *Hepatol Int*. 2024;18(1):73–90. doi:10.1007/s12072-023-10615-9
9. Zheng Y, Han Y, Sun Q, Li Z. Harnessing anti-tumor and tumor-tropism functions of macrophages via nanotechnology for tumor immunotherapy. *Exploration*. 2022;2(3):20210166. doi:10.1002/EXP.20210166
10. Yang M, Wang B, Hou W, et al. NAD + metabolism enzyme NNMT in cancer-associated fibroblasts drives tumor progression and resistance to immunotherapy by modulating macrophages in urothelial bladder cancer. *J Immunother Cancer*. 2024;12:e009281. doi:10.1136/jitc-2024-009281
11. Ji Y, Tan H, Cheng X, et al. Targeting JAK2/STAT3-dependent macrophage polarization by chlorogenic acid attenuates hepatic inflammation in chronic stress. *Cells*. 2025;14:1848. doi:10.3390/cells14231848
12. Nong F, Xing S, Cheng W, Deng S. Zuojin wan suppresses the progression of colorectal cancer by inhibiting M2 tumor-associated macrophages through JAK2/STAT3 signaling pathway and in vivo and in vitro. *Integrative Cancer Therapies*. 2025;24:15347354251375951. doi:10.1177/15347354251375951
13. Su P, Yu T, Zhang Y, et al. Upregulation of MELK promotes chemoresistance and induces macrophage M2 polarization via CSF-1/JAK2/STAT3 pathway in gastric cancer. *Cancer Cell Int*. 2024;24:287. doi:10.1186/s12935-024-03453-8
14. Huang X, Lin R, Liu H, et al. Resatorvid (TAK-242) ameliorates ulcerative colitis by modulating macrophage polarization and T helper cell balance via TLR4/JAK2/STAT3 signaling pathway. *Inflammation*. 2024;47:2108–2128. doi:10.1007/s10753-024-02028-z
15. Liang Y, Li J, Yuan Y, et al. Exosomal miR-106a-5p from highly metastatic colorectal cancer cells drives liver metastasis by inducing macrophage M2 polarization in the tumor microenvironment. *J Exp Clin Cancer Res*. 2024;43:281. doi:10.1186/s13046-024-03204-7
16. Jin Y, Kang Y, Wang M, et al. Targeting polarized phenotype of microglia via IL6/JAK2/STAT3 signaling to reduce NSCLC brain metastasis. *Signal Transduction Targeted Ther*. 2022;7(52). doi:10.1038/s41392-022-00872-9
17. Yun J, Zhang Y, Zhang H, et al. Anti-inflammatory properties of *Pleione bulbocodioides* extract through STING/NF-κB pathway inhibition. *Mol Immunol*. 2025;183:83–92. doi:10.1016/j.molimm.2025.04.015
18. Yang Y, Li L, Yu D, et al. A naturally occurring phenanthrene from *Pleione bulbocodioides* inhibits osteoclast formation by directly targeting src kinase. *Eur J Pharmacol*. 2025;1002:177854. doi:10.1016/j.ejphar.2025.177854
19. Wang Y, Kong H, Huang R, et al. Elucidating the structures and antitumor activities of *Pleione bulbocodioides* polysaccharides. *Int J Biol Macromol*. 2025;332:148532. doi:10.1016/j.ijbiomac.2025.148532
20. Li J, Liu Z, Wu X, et al. Anti-metastatic effects of AGS-30 on breast cancer through the inhibition of M2-like macrophage polarization. *Biomed Pharmacother*. 2024;172:116269. doi:10.1016/j.biopha.2024.116269
21. Tang C, Jiang S-T, Li C-X, Jia X-F, Yang W-L. The effect of salvianolic acid a on tumor-associated macrophage polarization and its mechanisms in the tumor microenvironment of triple-negative breast cancer. *Molecules*. 2024;29(7):1469. doi:10.3390/molecules29071469
22. Liu Y, Yang J, Guo Z, et al. Immunomodulatory effect of *Cordyceps militaris* polysaccharide on RAW 264.7 macrophages by regulating MAPK signaling pathways. *Molecules*. 2024;29:3408. doi:10.3390/molecules29143408
23. Yue H, Xu Q, Li X, et al. Physicochemical characterization and immunomodulatory activity of a novel acid polysaccharide from solanum muricatum. *Polymers*. 2019;11:1972. doi:10.3390/polym11121972
24. Han Z, Yang D, Trivett A, Oppenheim JJ. Therapeutic vaccine to cure large mouse hepatocellular carcinomas. *Oncotarget*. 2017;8(32):52061–52071. doi:10.18632/oncotarget.19367
25. Fei S, Li W, Xiang L, Xie X, Zhang L. Protective effect of alprostadil on acute pancreatitis in rats via inhibiting janus kinase 2 (JAK2)/STAT3 signal transduction pathway. *Med Sci Monitor*. 2019;25:7694–7701. doi:10.12659/MSM.919148
26. Fang Y, Ning A, Li S, et al. Polysaccharides extracted from rhizoma pleionis have antitumor properties in vitro and in an H22 mouse hepatoma ascites model in vivo. *Int J Mol Sci*. 2018;19:1386. doi:10.3390/ijms19051386
27. Charan J, Kantharia ND. How to calculate sample size in animal studies? *J Pharmacol Pharmacotherape*. 2013;4(4):303–306. doi:10.4103/0976-500X.119726
28. Arifin WN, Zahiruddin WM. Sample size calculation in animal studies using resource equation approach. *Malaysian J Med Sci*. 2017;24(5):101–105. doi:10.21315/mjms2017.24.5.11
29. Chen S, Saeed AF, Liu Q, et al. Macrophages in immunoregulation and therapeutics. *Signal Transduction Targeted Ther*. 2023;8:207.
30. Fu X, Pang M, Wang Z, Wang H. Macrophage polarization in the tumor microenvironment of hepatocellular carcinoma: from mechanistic insights to translational therapies. *Cancer Control*. 2025;32:10732748251406674. doi:10.1177/10732748251406674
31. Song S, Shi K, Fan M, et al. Clostridium butyricum and its metabolites regulate macrophage polarization through miR-146a to antagonize gouty arthritis. *J Adv Res*. 2026;80:943–960. doi:10.1016/j.jare.2025.05.036
32. Zheng Y, Wang N, Wang S, et al. Chronic psychological stress promotes breast cancer pre-metastatic niche formation by mobilizing splenic MDSCs via TAM/CXCL1 signaling. *J Exp Clin Cancer Res*. 2023;42:129. doi:10.1186/s13046-023-02696-z
33. Zhao H, Wu L, Yan G, et al. Inflammation and tumor progression: signaling pathways and targeted intervention. *Signal Transduction Targeted Ther*. 2021;6:263.
34. Chen Y, Hou C, Yang N, et al. Regulatory effect of JAK2/STAT3 on the immune function of endotoxin-tolerant dendritic cells and its involvement in acute liver failure. *J Clin Transl Hepatol*. 2022;10:879–890. doi:10.14218/JCTH.2021.00175
35. Zhou M, Zhang Y, Zhang Q, Tong Y. METTL14-mediated m6A modification upregulated SOCS3 expression alleviates thyroid cancer progression by regulating the JAK2/STAT3 pathway. *Mol Cell Probes*. 2024;78:101987. doi:10.1016/j.mcp.2024.101987
36. Hu Z, Sui Q, Jin X, et al. IL6-STAT3-C/EBPβ-IL6 positive feedback loop in tumor-associated macrophages promotes the EMT and metastasis of lung adenocarcinoma. *Exp Clin Cancer Res*. 2024;43:63. doi:10.1186/s13046-024-02989-x
37. Liao Q, Zhou X, Wu L, et al. Gut microbial metabolite 4-hydroxybenzeneacetic acid drives colorectal cancer progression via accumulation of immunosuppressive PMN-MDSCs. *J Clin Invest*. 2025;135:e181243. doi:10.1172/JCI181243
38. Zhang Z, Yu Y, Zhang Z, et al. Cancer-associated fibroblasts-derived CXCL12 enhances immune escape of bladder cancer through inhibiting P62-mediated autophagic degradation of PDL1. *J Exp Clin Cancer Res*. 2023;42:316. doi:10.1186/s13046-023-02900-0

39. Liu Y, Jiao X, Meng X, et al. Hepatotoxicity of 8:2 polyfluoroalkyl phosphate diesters exposure via JAK2/STAT3 pathway activation and M1 macrophage polarization in mice. *Environ Sci Technol*. 2025;59:19185–19194. doi:10.1021/acs.est.5c06681
40. Tang Y, Deng X, Wang Y, et al. NSUN2-mediated m5C modification of SOCS3 mRNA modulates macrophage polarization in bladder cancer. *Cell Death Dis*. 2025;17:75. doi:10.1038/s41419-025-08306-4
41. Xie L, Liu G, Huang Z, et al. Tremella fuciformis polysaccharide induces apoptosis of B16 melanoma cells via promoting the M1 polarization of macrophages. *Molecules*. 2023;28:4018. doi:10.3390/molecules28104018
42. Chen S, Wang B, Xue Q, et al. Selenium-modified polysaccharide from acanthopanax senticosus enhances anti-tumour immunity through gut microbiota modulation. *Phytomed*. 2026;150:157704. doi:10.1016/j.phymed.2025.157704
43. Shi D, Xu X, Wang J, et al. Synergistic anti-inflammatory effects of ganoderma lucidum polysaccharide and ganoderic acid a on LPS-induced RAW264.7 cells by inhibition of TLR4/NF-κB activation. *Int J Biol Macromol*. 2025;309:143074. doi:10.1016/j.ijbiomac.2025.143074
44. Zhang D, Wei Y, Zhu X, et al. Study on the intervention mechanism of ganodermalucidum polysaccharides in mice with atopic dermatitis. *Food Res Int*. 2025;221:117212. doi:10.1016/j.foodres.2025.117212
45. Cui Z, Shang Q. Mechanistic insights into the antitumor effects of astragaloside IV and astragalus polysaccharide in digestive system cancers. *Front Pharmacol*. 2025;16:1691011. doi:10.3389/fphar.2025.1691011
46. Liu X, Guo C, Yang W, et al. Composite microneedles loaded with astragalus membranaceus polysaccharide nanoparticles promote wound healing by curbing the ROS/NF-κB pathway to regulate macrophage polarization. *Carbohydr Polym*. 2024;345:122574. doi:10.1016/j.carbpol.2024.122574
47. Liu D, Zhu Y, Hou Z, Wang H, Li Q. Polysaccharides from astragalus membranaceus bunge alleviate LPS-induced neuroinflammation in mice by modulating microbe-metabolite-brain axis and MAPK/NF-κB signaling pathway. *Int J Biolog Macromole*. 2025;304:140885. doi:10.1016/j.ijbiomac.2025.140885
48. Wang W, Wang J, Wu N, et al. Algal β-glucan: structure, immunomodulatory effects and application prospects. *Carbohydr Polym*. 2026;376:124801. doi:10.1016/j.carbpol.2025.124801
49. Wang B, Wu B, Ma Y, et al. Astragalus polysaccharides: structure-immunomodulation relationships, multi-target pharmacological activities, and cutting-edge applications in immune modulation. *Front Immunol*. 2025;16:1714898. doi:10.3389/fimmu.2025.1714898